ACS NANO

www.acsnano.org

ARTICLE

Interfacial Polymerization Depth Mediated by the Shuttle Effect Regulating the Application Performance of Pesticide-Loaded Microcapsules

Tao Zhang, Hongzhen Sun, Liyuan Yang, Peng Zhang, Yaozhong Zhang, Jingbo Bai, Feng Liu,* and Da-xia Zhang*

Cite This: https://doi.org/10.1021/acsnano.3c07915

Read Online

ACCESS | Metrics & More | Article Recommendations | Supporting Information

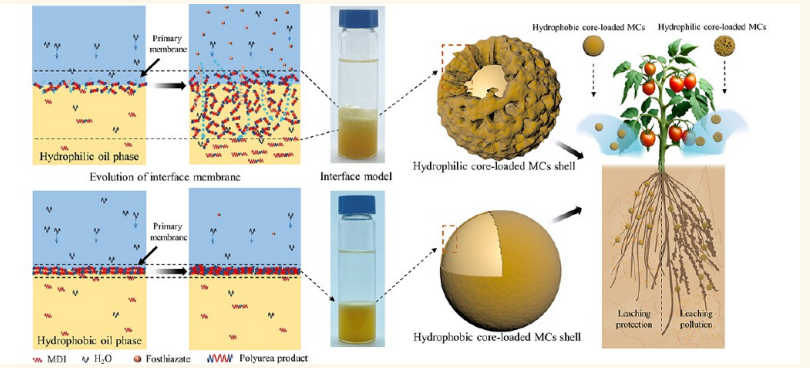

ABSTRACT: **The highly water-soluble nematicide fosthiazate is anticipated to undergo microencapsulation in order to enhance its retention around plant roots and mitigate leaching into groundwater. However, the underlying mechanism governing the influence of hydrophilicity of the microcapsule (MC) core on the evolution of the microcapsule shell remains unclear, posing challenges for encapsulating water-soluble core materials. This study elucidates the microlevel formation mechanism of microcapsules by investigating the impact of interfacial mass transfer on shell formation and proposes a method for regulating the structure of shells. The study reveals that enhancing the hydrophilicity of the core enhances the shuttle effect between the oil and aqueous phase, expands the region of polymerization reactions, and forms a loose and thick shell. The thickness of the microcapsule shell prepared using solvent oil 150# (MCs-SOL) measures only 264 nm, while that of the microcapsules prepared using propylene glycol diacetate and solvent oil 150# at a ratio of 2:1 (MCs-P2S1) is 5.2 times greater. The enhanced compactness of the shell reduced the release rate of microcapsules and the leaching distance of fosthiazate in soil, thereby mitigating the risk of leaching loss and facilitating the distribution of active ingredients within crop roots. The MCs-SOL had a limited leaching distance measurement of 8 cm and exhibited a satisfactory efficacy of 87.3% in controlling root galling nematodes. The thickness and compactness of the MCs shell can be regulated by manipulating the interfacial shuttle effect, providing a promising approach to enhancing utilization efficiency while mitigating potential environmental risks.**

KEYWORDS: *nematicide, fosthiazate, hydrophilicity solvent, interface shuttle, utilization, leaching*

INTRODUCTION

A substantial number of pesticides are applied to the soil to mitigate the detrimental impact caused by soil-borne diseases and parasitic nematodes on crops.[1,2] To ensure the satisfactory crop yield and reduce the workload of pesticide applied, farmers often resort to excessive pesticide usage.[3,4] Simulta-

Received: August 22, 2023
Accepted: October 4, 2023

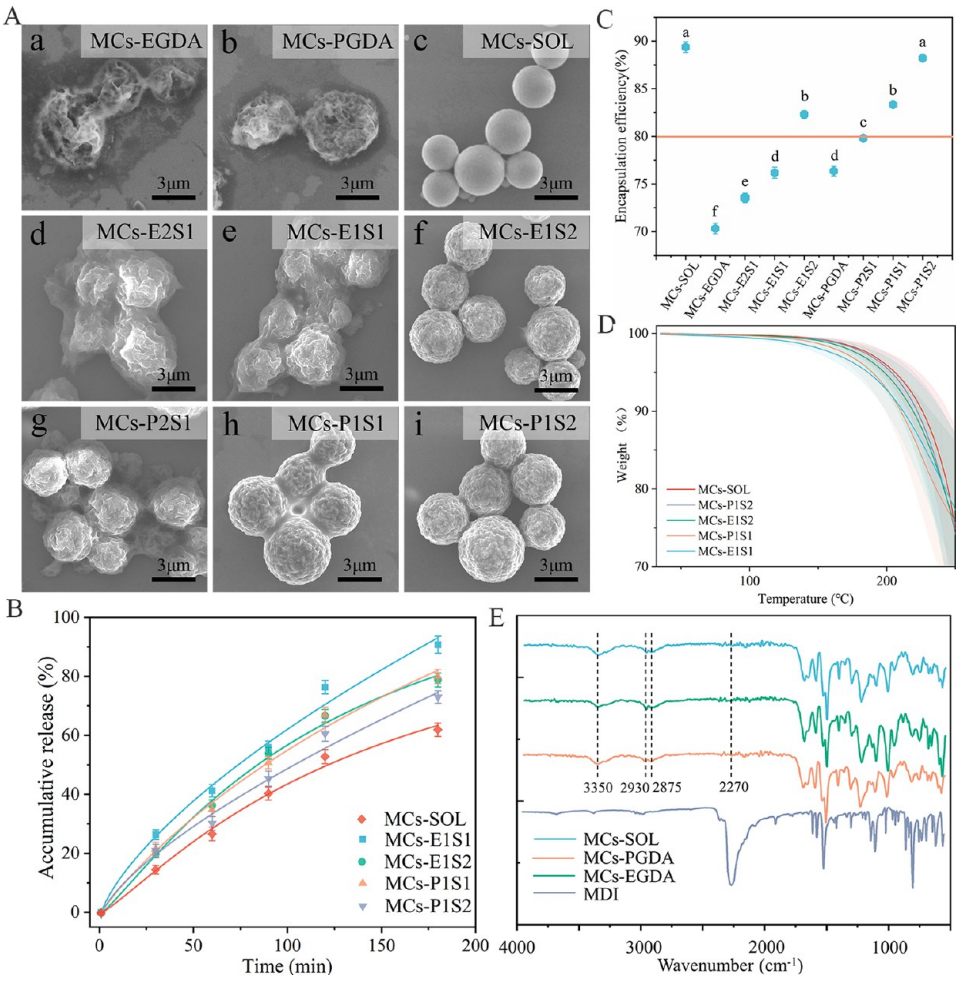

Figure 1. (A) Morphology of fosthiazate-loaded MCs. (B) Release profiles of fosthiazate-loaded MCs. (C) Encapsulation efficiency of fosthiazate-loaded MCs. (D) TGA curves of fosthiazate-loaded MCs. (E) FTIR spectra of the shells of fosthiazate-loaded MCs.

neously, achieving a uniform distribution of soil-applied pesticides is crucial for enhanced interaction with harmful organisms and pesticides.[5,6] Pesticides with high water solubility are more likely to be evenly distributed within the soil facilitated by irrigation or precipitation events. However, the application of these pesticides poses a potential contamination risk to groundwater.[7,8] Currently, microencapsulation technology is regarded as a promising solution for mitigating leaching pollution caused by pesticides, improving pesticide utilization efficiency, and ensuring environmental safety.[9−11] However, the preparation instability and the absence of stability control strategies have presented challenges for promoting and implementing this technology for microencapsulation of highly water-soluble pesticides.

After being invaded by root galling nematodes, the host plant was stimulated to form root nodules, thereby impacting crop yield and quality.[12,13] Among these hazards, *Meloidogyne incognita* is particularly prevalent in China and poses the greatest threat to vegetable cultivation.[14,15] Therefore, the application of nematicides is imperative for controlling nematode damage. Fosthiazate, an organophosphorus nematicide with a solubility of 9 g/L in water, is globally employed for the control of *M. incognita*.[16,17] However, the International Union of Pure and Applied Chemistry (IUPAC) has classified fosthiazate as a pesticide with a high leaching potential. Therefore, the implementation of effective measures, such as microencapsulation, is imperative to mitigate the environmental risks associated with fosthiazate. Currently, registered microcapsule (MC) preparations containing 20% and 30% fosthiazate are utilized for the management of root galling nematodes in China. It has been reported that two methods of in situ and interfacial polymerization were employed to prepare fosthiazate-loaded MCs.[18,19] Presently, interfacial polymerization stands as the most industrialized technology for microencapsulation because it possesses advantages of simple process, fast reaction rate, and suitability for continuous production.[20−22] However, there is currently a dearth of straightforward and efficacious methodologies for encapsulating fosthiazate to obtain a stable preparation. Achieving complete encapsulation is crucial for fabricating microcapsule preparation, enabling controlled release of the core material, and effectively enhancing application efficacy.[23,24]

The formation of MCs through interfacial polymerization involves two sequential processes: emulsion generation and interfacial membrane formation. The formation of the membrane was through a condensation reaction between oil phase and aqueous phase monomers at the oil-aqueous interface, resulting in the development of core−shell pesticide-loaded particles. Moreover, there is limited research on elucidating the mechanism underlying shell formation.[25,26] The construction of the interfacial membrane begins with the diffusion of the aqueous monomer into the oil phase, followed

https://doi.org/10.1021/acsnano.3c07915
ACS Nano XXXX, XXX, XXX−XXX

by polymerization and cross-linking with another monomer.[27−29] Nevertheless, there are divergent viewpoints regarding the growth mechanism of the interfacial membrane. The first hypothesis proposed the initial development of a primary membrane, followed by subsequent growth on the oil phase side to establish an interfacial membrane.[26,27] The second hypothesis indicated that the monomer diffused from the aqueous phase into the oil phase, where it associated with other monomers present in the oil phase to form oligomeric nanoclusters. Subsequently, these nanoclusters undergo aggregation and precipitation upon reaching their solubility limit, forming a high polymer. Despite varying interpretations of interface membrane formation, it was widely acknowledged that mass transfer played a crucial role in this process. For instance, the introduction of *n*-hexadecane into the oil phase, which exhibited lower water solubility compared to decalin, leading to a reduction in pore size and thinning of the interface membrane.[30] Currently, this method is widely employed for encapsulating pesticides with lipid solubility, such as chlorpyrifos and L-cypermethrin.[31,32] The encapsulation of water-soluble materials has been a formidable challenge. During the microencapsulation of pesticides with high water solubility, the hydrophilicity of the oil phase may promote substance exchange between the oil and aqueous phases at the interface layer, thereby influencing the formation of shell. Currently, there is a paucity of literature addressing the underlying mechanism and strategy for enhancing the encapsulation efficiency of water-soluble materials.

In this study, interfacial mass transfer was employed as a breakthrough point to clarify the relationship between the water solubility of the MCs core and the formation of MCs. Fosthiazate-loaded MCs were prepared by adjusting the hydrophilicity and hydrophobicity of the core-used solvents, establishing a correlation between shell microstructure and preparation stability. And a interface evolution model was developed to reveal the underlying mechanism governing the influence of oil phase hydrophilicity/hydrophobicity on membrane structure. This study aims to enrich the existing microencapsulation theory of interfacial polymerization and provide suggestions for the encapsulation of water-soluble materials. The subsequent research will investigate the impact of viscosity, temperature, hydrophobic materials, and other factors that impede mass transfer on the encapsulation process of water-soluble pesticides.

RESULTS AND DISCUSSION

Particle Size Distribution and Morphology of Fosthiazate-Loaded MCs. The particle-size distributions of fosthiazate-loaded MCs fabricated by using various solvents were similar, as shown in Figure S1. This advantageous similarity helps to mitigate the impact of particle sizes on the performance of MCs. The morphology of MCs is shown in Figure 1A. The particles of MCs-EGDA (EGDA = ethylene glycol diacetate) and MCs-PGDA (PGDA = propylene glycol diacetate) exhibited distinct interconnection and collapse (Figure 1A-a,A-b). Nevertheless, the particles of MCs-SOL (SOL = solvent oil 150#) exhibited a spherical morphology (Figure 1A-c). Therefore, employing a solvent with low hydrophilicity was beneficial for obtaining a smooth and continuous membrane. Six types of fosthiazate-loaded MCs, with cores exhibiting varying degrees of hydrophilicity, were prepared by adjusting the proportions of SOL, EGDA, and PGDA to further evaluate the effect of solvent hydrophilicity on the morphology of the MCs (Figure 1A-d∼A-i). The morphology of the MCs underwent a transition to a collapsed, adhesive, and wrinkled state as the proportion of hydrophilic solvent increased. These different morphologies of the MCs demonstrate the discrepancies in the shell structure, which subsequently influence encapsulation efficiencies and release profiles.[33,34]

Encapsulation Efficiency. The encapsulation efficiencies of fosthiazate-loaded MCs samples with various core solvents are illustrated in Figure 1C. The encapsulation efficiencies of the five samples, which contained a high proportion of hydrophobic solvents, exceeded 80%. The encapsulation efficiencies of the MCs-SOL and MCs-P1S2 samples were 89.37% and 88.21%, respectively, which were significantly higher compared to the other samples. Increasing the proportion of hydrophobic solvent in the oil phase, regardless of whether the MCs samples were prepared using a single or mixed solvent, confers advantageous effects on enhancing encapsulation efficiency.

Simultaneously, it is intriguing to observe significant alterations in the viscosity and encapsulation efficiency of the preparation after thermal storage (Figure S2). After 14 days of thermal storage, the viscosity change of the MCs-SOL sample was the smallest with an increase of only 21 mPa/s (Figure S2A). Correspondingly, the viscosity of the other samples increased in the range of 25−85 mPa/s. Negligible changes in the encapsulation efficiency of the MCs-SOL sample were observed following thermal storage (Figure S2B). Notably, the enhanced hydrophilicity of the MCs core resulted in an increase in viscosity and a decrease in the encapsulation efficiency of the preparation following thermal storage. After 30 days of thermal storage, severe agglomeration was evident in MCs-EGDA, MCs-PGDA, MCs-E2S1, and MCs-P2S1 samples (Figure S2C).

Release Profiles. The release profiles of MCs samples were evaluated and are presented in Figure 1B and Figure S3. MCs-SOL exhibited the slowest release rate, with a cumulative release proportion of 62.05% in 3 h. Within the same time frame, MCs-E1S1 demonstrated a cumulative release proportion of 89.85%, while MCs-E1S2 and MCs-P1S1 had proportions of 83.21% and 82.77%, respectively. The cumulative release proportion of MCs-E1S1 at 3 h exhibited a significant increase compared to that of MCs-P1S1, indicating an augmented presence of hydrophilic solvents within the core of MCs that enhanced the release rate of active ingredient. As we know, the release of MCs is influenced by factors of particle size, shell structure, and the diffusion coefficient of the core within the shell. Furthermore, the particle size distributions of various MCs investigated in this study were comparable. Therefore, the accelerated release of MCs researched in this study may be attributed to either the hydrophilic solvent promoting core diffusion or potential variations in the shell structure, which require further research and discussion.

Thermal Stability. The weight loss efficiency of the core material is generally influenced by the compactness of the shell.[34] As shown in Figure S4, the weight loss of fosthiazate-loaded MCs prepared by using various solvents was divided into two stages. The initial phase (below 250 °C) of weight loss was attributed to the loss of the core material, while the subsequent phase corresponds to the degradation of shell. The observed differences in the curves of each treatment did not reach statistical significance. However, based on the average

https://doi.org/10.1021/acsnano.3c07915
ACS Nano XXXX, XXX, XXX−XXX

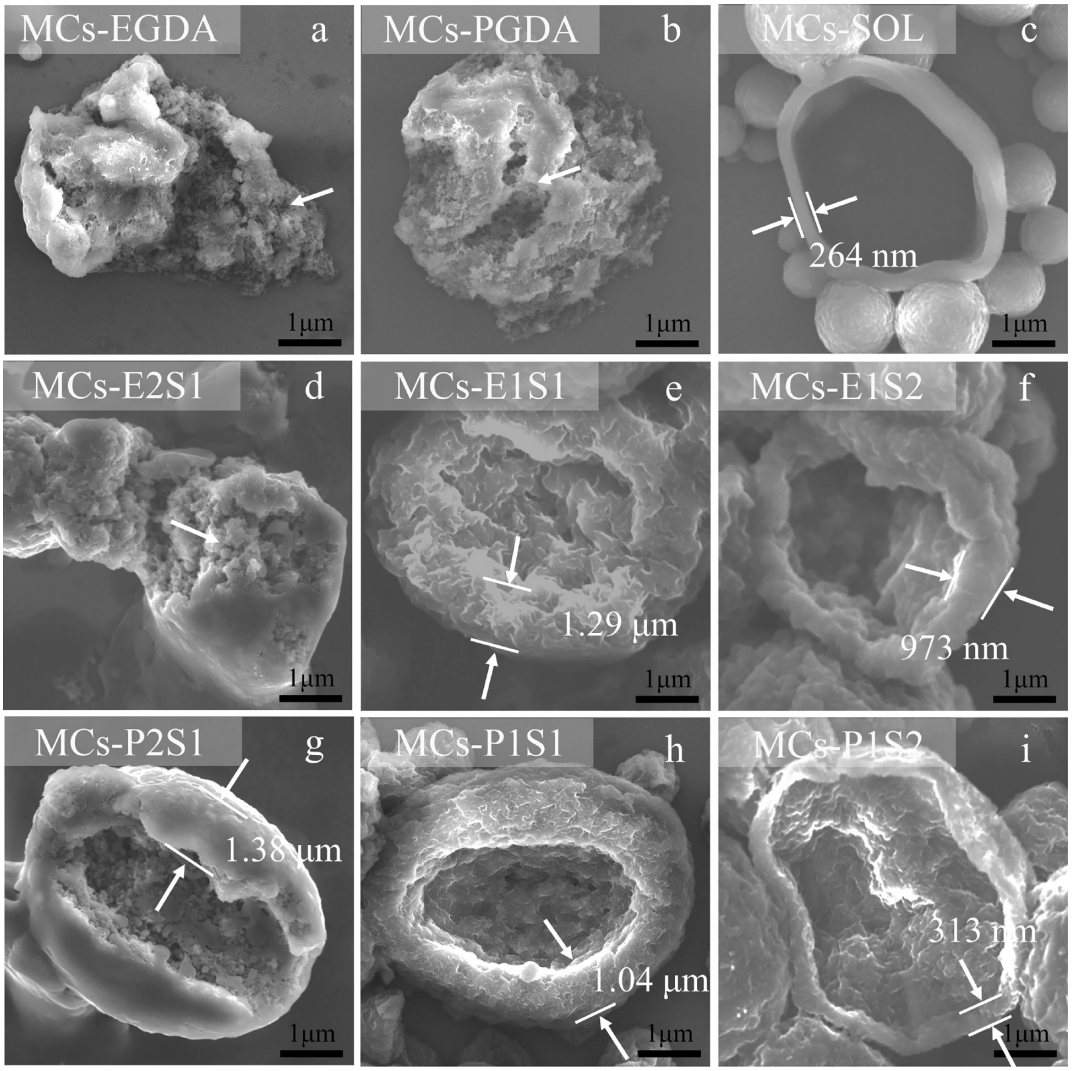

Figure 2. Morphology of the fosthiazate-loaded MCs shell prepared using various solvents.

data obtained from three experiments, it can be observed that the MCs-E1S1 sample exhibited the fastest weight loss rate, while the MCs-SOL sample demonstrated the slowest weight loss rate (Figure 1D). Consequently, considering both release and thermal stability results, we think that the hydrophilicity of a solvent exerted an influence on the compactness of the MCs shell.

Chemical Component Analysis of the MCs Shell. We attempted to reveal the differences in the release performance of various MCs from the perspective of the chemical structure of the carrier. The interfacial polymerization reaction formula in this study is shown in Figure S5. As shown in Figure 1E, the Fourier transform infrared (FTIR) spectra of the shells of MCs fabricated by using three solvents were basically consistent. The presence of isocyanate groups in 4,4-diphenylmethane diisocyanate (MDI) was evidenced by a strong absorption peak observed at 2270 cm^{-1}, while a reduction in this absorption peak across all three MCs indicated the occurrence of cross-linking. The characteristic peaks observed at 2875, 2930, and 3350 cm^{-1} indicated the existence of C−H stretching vibrations from the methyl and methylene groups as well as N−H stretching. The obtained results provide evidence for the occurrence of a polyurea reaction between MDI and water[25] as well as indicating that the solvent does not participate in shell formation.

Difference in the Internal Structure of MCs. The above results indicate that the increase in water solubility of the core leads to the decrease of the encapsulation efficiency and an acceleration of the release of the microcapsules, which may be the inducement of instability of the preparation. Given that the solvent in the core does not affect the chemical composition of the shell, our focus shifted toward investigating the microstructure of the shell. The structure of MCs shell was characterized by scanning electron microscopy (SEM) (Figure 2). The internal structure of MCs, along with the thickness and structure of the shell, exhibits a significant correlation with the presence of a water-soluble core. Among all samples, MCs-SOL displayed the thinnest shell (264 nm) with a relatively smooth surface (Figure 2-c). Notably, the shell thickness of MCs-P2S1 was approximately 5.2 times that of MCs-SOL. Moreover, with an increase in the hydrophilicity of the solvent, the shell exhibited thickening for MCs and even formed solid spheres (Figure 2a,b,d). However, this thickening did not impede the release rate of the core material, as evidenced by its release behavior in both liquid media and thermal environments. Notably, the MCs-SOL sample displayed the thinnest shell and the lowest release efficiency, which necessitates

https://doi.org/10.1021/acsnano.3c07915
ACS Nano XXXX, XXX, XXX−XXX

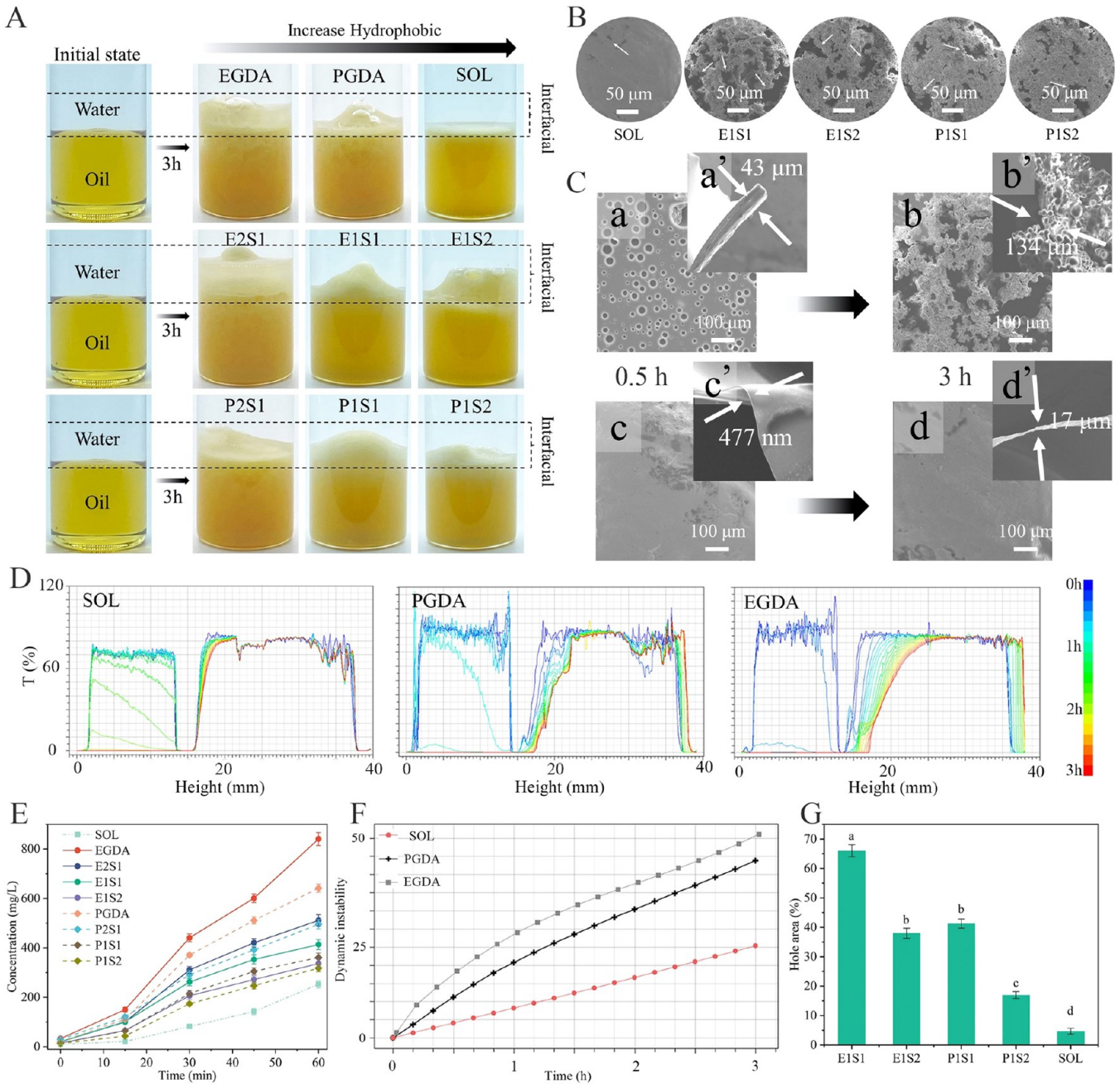

Figure 3. (A) Oil-aqueous interface evolution models formed using various solvents. (B) Characterization of the interfacial membrane of the oil-aqueous interface evolution model. (C) Evolution process of the interface membrane. (D) Changes in transmittance of oil-aqueous phase. (E) Concentration of fosthiazate detected at different times at the same position of aqueous phase. (F) Dynamic instability of the interface evolution model. (G) Hole area corresponding to the oil-aqueous interface models formed using different solvents.

further analysis of its microstructure and formation mechanism to elucidate the underlying reasons.

Mechanism of the Interface Membrane Formation. From the above results, the hydrophilicity of the MCs core exerts an influence on the formation of MCs. The formation of an interfacial membrane is a coupled chemical reaction including interfacial mass transfer, which involves complex mass transfer kinetics and polycondensation reactions. Hence, investigating the evolutionary mechanism of the membrane has always been a challenge. This research has established a simple method for macroscopically visualizing the microprocess of shell formation, thereby facilitating a deeper comprehension of the evolutionary dynamics of interfacial membranes.

The interface evolution model was employed to study the formation of an interface membrane and the factors that can be regulated including active ingredients (fosthiazate and phoxim with water solubility of 9 and 1.5 mg/L, respectively) and solvents (SOL, PGDA, and EGDA with water solubilities of 0, 90, and 160 g/L, respectively). When the oil phase contained fosthiazate along with EGDA and PGDA as solvents, the oil phase exhibited turbidity and the result appeared to have an insufficiently smooth interface membrane after a duration of 3 h (Figure S6). Conversely, the formation of a smooth interface membrane was facilitated by lipophilic active ingredients and solvents (Phoxim and SOL). Therefore, it can be inferred that

https://doi.org/10.1021/acsnano.3c07915
ACS Nano XXXX, XXX, XXX−XXX

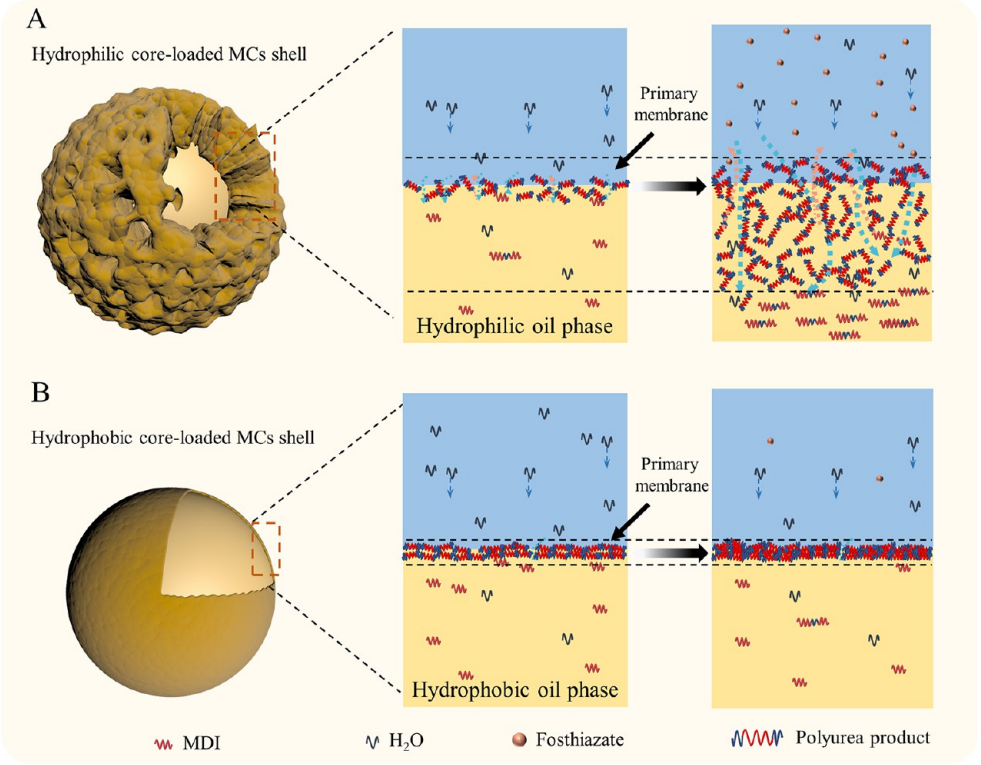

Figure 4. Schematic of interface membrane formation mechanism affected by the interface shuttling effect.

hydrophilic active ingredients are not conducive to maintaining stability at the oil-aqueous interface.

The formulation was incorporated into the model based on Table S2. There is a significant correlation between the color, transmittance, volume, and interface membrane morphology of the oil phase and water-soluble solvents (Figure 3A). Notably, the turbidity and volume of the oil phase increased with the hydrophilicity of the solvent. This is responsible for the infiltration of water into the oil phase and reaction with MDI. Therefore, enhancing the hydrophilicity of the oil phase led to a greater depth of interfacial polymerization and a thicker interfacial membrane. The turbiscan was used to scan and record variations in the optical signals of the system within the interface model. When EGDA and PGDA were utilized as solvents for the oil phase, the transmittance of the oil phase decreased to 0 after 31 and 50 min, respectively (Figure 3D). Simultaneously, the oil phase completely turned into an opaque solid after a 3 h reaction. In contrast, when SOL served as the solvent for the oil phase, full opacity was achieved after 130 min. The Movies S1, S2, and S3 exhibited the variation in transmittance of the oil-aqueous phase, illustrating that a higher hydrophilicity of the oil phase led to a shorter duration of sustained transmittance. This observation indicates that the hydrophobic nature of the oil phase hindered water diffusion toward it, thereby reducing the depth at which interfacial reactions occur. In addition, this result is consistent with the findings of MCs morphology, where the increasing water solubility of the oil phase induced an augmentation in shell thickness and even transformed the core−shell structure into a solid sphere.

The dynamic instability coefficient serves as evidence supporting this result. In stability analysis, the dynamic instability coefficient was employed as an indicator to describe the dynamic stability of a system. It reflected whether the system could produce irreversible and amplified responses when subjected to small disturbances. In the interface evolution model, the dynamic instability coefficient increased as the solvent hydrophilicity in the oil phase was enhanced (Figure 3F). The enhanced hydrophilicity of the oil phase resulted in increased interfacial instability, thereby influencing the formation of the interfacial membrane.[35,36]

Interface Shuttling Effect Verification. The turbidity of the oil phase indicates the ingress of water into the oil phase during formation of the interface membrane. Additionally, the oil phase itself has a certain degree of water solubility, raising a question regarding whether oil can also enter the aqueous phase during interface membrane formation. The changes in the concentration of fosthiazate were detected at different time points within the same aqueous phase position (Figure 3E). When EGDA or PGDA was employed as the oil-phase solvent, the concentration of fosthiazate detected was the highest at each time point. However, when SOL was used as the solvent, the concentration of fosthiazate after 60 min was significantly lower compared to other samples, at 252.8 mg/L. This indicates that the hydrophobic oil phase can hamper the entry of fosthiazate into the aqueous phase. Therefore, the aqueous phase can enter the oil phase and the hydrophilic oil phase can enter the aqueous phase. And the efficiency of mass transfer from the oil phase to the aqueous phase positively correlates with the hydrophilicity of the oil phase. The process of shuttling oil and water at the interface is defined as the "interface shuttling effect". The interface shuttle effect can influence the contact efficiency and extent of polycondensation reaction between water and MDI, thereby influencing the formation of the interface membrane.

Compactness of the Interfacial Membrane. To investigate the influence of the interface shuttle effect on the interface membrane, the morphology of the interface

https://doi.org/10.1021/acsnano.3c07915
ACS Nano XXXX, XXX, XXX−XXX

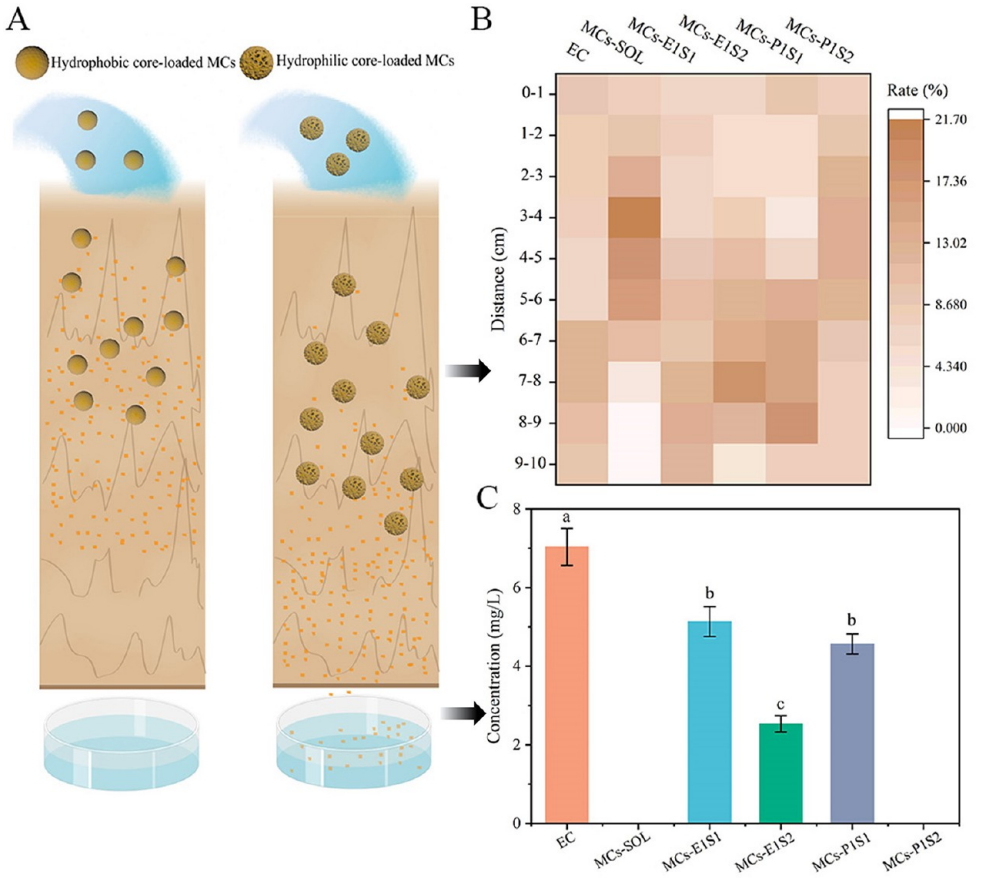

Figure 5. (A) Schematic of the mobility of fosthiazate in soil. (B) Mobility of fosthiazate in soil. (C) Concentration of fosthiazate in leachates.

membrane formed using various solvents that dissolved fosthiazate and MDI was analyzed. Figure 3B illustrates the morphology of the interface membrane, while Figure 3G shows the area occupied by interface membrane pores. There are pores present on each interface membrane, with the pore area in the SOL-induced interface membrane accounting for 4.77%. However, when E1S1 and P1S1 were employed as solvents, the pore areas in the interface membrane were 14.3 and 8.8 times larger than that of the SOL treatment, respectively. Therefore, the area of the pores gradually increased as the hydrophilicity of the solvent increased.

Evolution Process of the Interface Membrane. To explain the underlying mechanism through which different solvents exert influence on the MCs structure, the evolution of the interfacial membrane using solvents SOL and E1S1 as the oil phase was investigated by using an interfacial evolution model (Figure 3C). The thicknesses of the primary interface membranes formed using E1S1 and SOL were 43 μm and 477 nm, respectively, within the initial 30 min (Figure 3C-a' and Figure 3C-c'). The interfacial membrane formed by using E1S1 extended into the oil phase, and its thickness increased to 134 μm after 3 h. The primary interface membrane formed by using E1S1 exhibited many regular circular holes, whereas the primary interface membrane formed by using SOL appeared smooth and continuous. Moreover, these holes gradually enlarged and became irregular over time, leading to the formation of a porous and unsmooth interfacial membrane. In contrast, the interfacial membrane formed by using SOL maintained its thinness and compactness. This is consistent with the findings of the MCs shell structures formed by using various hydrophilic solvents. The influence of the interface shuttle effect becomes more pronounced as the core's hydrophilicity increases. The interface shuttle effect significantly influenced the contact between MDI and water, while the polycondensation reaction at the oil-aqueous interface extends from the water phase to the oil phase, resulting in the formation of a thick, porous shell.

Formation Mechanism of Interface Membrane. Based on the above results, we employed the schematic shown in Figure 4 to reveal the underlying mechanism governing the influence of hydrophilic components in the oil phase on the formation of MCs structures through interfacial polymerization. The process of interfacial polymerization involves a nonequilibrium mass transfer process coupled with rapid chemical reactions. Following the initiation of the interfacial polycondensation reaction, the liquid−liquid interface undergoes a swift transformation to a liquid−solid−liquid interface. As shown in Figure 4A, when the oil phase was a hydrophilic system, there was a substance exchange between the aqueous phases and oil phases at the interface. The monomers diffuse from the aqueous phase into the oil phase and rapidly react with MDI, resulting in the formation of a primary interfacial membrane. At this stage, the interfacial membrane exhibits discontinuity, resulting in irregular perforations. Monomers from the aqueous phase permeate through the interfacial membrane into the oil phase and continue participating in the reaction. The hydrophilic nature of the oil phase enhances both the diffusion rate and penetration depth of aqueous-phase

https://doi.org/10.1021/acsnano.3c07915
ACS Nano XXXX, XXX, XXX−XXX

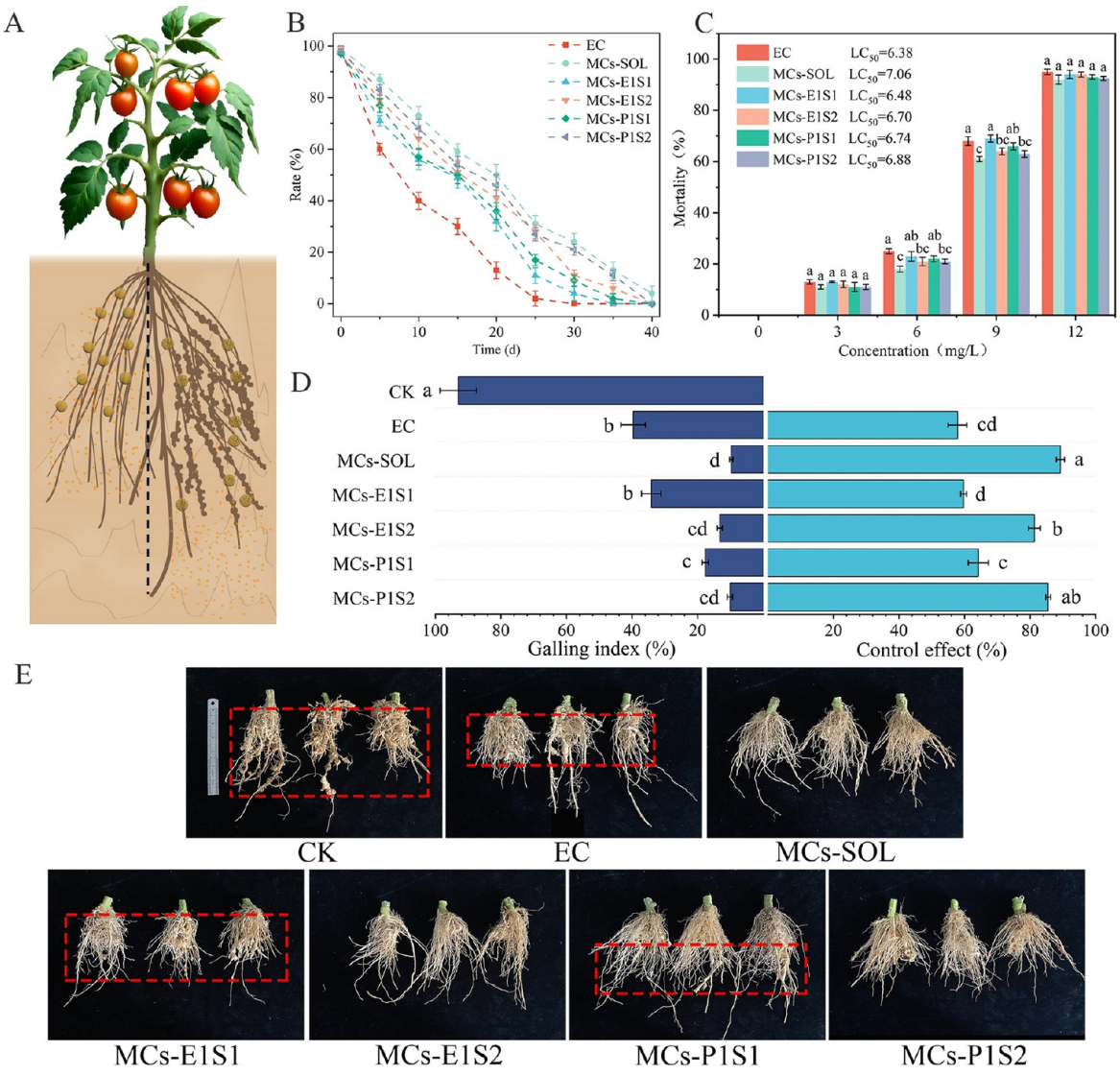

Figure 6. (A) Schematic of MCs distribution in the roots of tomato. (B) Degradation of fosthiazate in soil. (C) Nematicidal activity of fosthiazate-loaded MCs. (D) Root galling index and the control effect of fosthiazate-loaded MCs on roots for 90 days. (E) Incidence of root galling nematode disease under different treatments at 90 days.

monomers toward the oil phase. Eventually, the diffusion of aqueous-phase monomers decelerates and ceases, thereby facilitating the formation of a porous and loosely structured interface membrane. When the oil phase had a hydrophobic property (Figure 4B), the interfacial polycondensation reaction mainly relied on the molecular diffusion of aqueous monomer into the shallow layer of oil phase for chemical reactions. This is similar to a prototypical Freger model,[29] thereby resulting in a decelerated or halted water diffusion rate toward the oil phase. As a result, a smooth, continuous, and thin interfacial membrane is formed. Consequently, the structural characteristics of the MCs shell can be modulated by the water solubility of the oil phase, thereby exerting a significant influence on both stability and application performance of MCs preparation.

Mobility of Fosthiazate in Soil. The efficacy of fosthiazate in controlling root galling nematode diseases can be influenced by its mobility and duration in soil. Therefore, the shell structure of fosthiazate-loaded microcapsules plays a crucial role in determining their performance (Figure 5A). In a previously published study, we had confirmed that the mobility range of MCs was contingent upon their particle size.[37,38] Notably, nanocapsules exhibited significant promotion for the mobility of pesticides in soil compared to microcapsules. In this study, we prepared MCs with consistent particle sizes in the micron range. Hence, the leaching distance of the fosthiazate in soil was solely determined by the characteristics of the active ingredient and the release rate of MCs.

The ideal nematocides were anticipated to exhibit prolonged persistence within the designated soil layer. In order to increase the concentration of abamectin around roots, hydrophilic modification was employed to mitigate the adsorption of abamectin by soil.[39] In contrast, fosthiazate needs to reduce its mobility in soil due to its higher solubility in water. The mobility of fosthiazate microencapsulated in soil was evaluated in this study by detecting the concentration of fosthiazate across different soil layers and leachate (Figure 5B,C and Table S3). Compared to MCs, the concentrations of fosthiazate were found to be higher within the depth range 6–10 cm in the EC samples, and the leachate exhibited the highest concentration. The fosthiazate of EC and MCs-E1S1

https://doi.org/10.1021/acsnano.3c07915
ACS Nano XXXX, XXX, XXX−XXX

samples predominantly accumulated in the middle and lower sections of the soil column. The fosthiazate concentration of the EC and MCs-E1S1 samples was significantly higher than that in other samples at a distance of 10 cm. The fosthiazate of the MCs-SOL sample could be detected at the deepest point of 8 cm, while the concentration of fosthiazate exhibited a significantly higher level compared to other samples within the depths of 4−6 cm. The MCs-SOL and MCs-E1S2 samples were not detected in the leachate. It is worth noting that the particle size distribution of the MC samples prepared in this study ranges from 1 to 6 μm. Therefore, during the leaching process of MC particles in soil, the soil acts as a filtering medium, allowing MC particles to remain in the upper soil layer. Meanwhile, due to its high water solubility, fosthiazate was easily leached to deep soil by water and transported over a long distance. Therefore, the compactness of the shell influenced the release efficiency of fosthiazate in MCs, resulting in differences in the detected concentrations of fosthiazate in various soil layers.

Degradation of Fosthiazate in Soil. To verify the variation in the duration of MCs samples prepared using various cores, the concentrations of fosthiazate in soil were detected within 40 days for each of the six samples (Figure 6B and Figure S7). After 30 days, the concentration of fosthiazate of the EC sample reached zero, while those of the other MCs samples exhibited significantly higher levels. The reduction in the hydrophilicity of the MCs core led to an extended persistence for fosthiazate in soil. The encapsulation of fosthiazate can enhance its resistance against soil interference, thereby improving its efficacy. The degradation pattern corresponds to the release pattern, indicating the degradation of the active ingredient following release within the soil.

The Control Efficacy of Fosthiazate-Loaded MCs to the Tomato Root Galling Nematodes Disease. The results of the nematicidal activity experiment are shown in Figure 6C. The mortality of the EC treatment group was slightly higher compared to all MC samples, while no statistical difference was observed among the various MCs samples. Therefore, it can be inferred that the variations observed in the control efficacies of MCs samples in the field trial may be attributed to the duration and mobility of fosthiazate in soil.

To verify the control efficacy of the MCs samples prepared using various solvents against root galling nematodes, field experiments were conducted (Figure 6D,E). As shown in Figure 6E, root galling, treated with EC and MCs-E1S1, was primarily observed in the upper and middle sections of the roots (Figure 6E). This observation can be attributed to the leaching of fosthiazate into deeper soil layers. As a result, their control efficacies against tomato root galling nematodes disease were only 57.8% and 59.7%, respectively. Nevertheless, the control efficacies of MCs-SOL and MCs-P1S2 treatments reached 87.3% and 83.5%, respectively (Figure 6D). It can be seen that the enhanced shell compactness led to a delayed release of fosthiazate, thereby mitigating its degradation and leaching in the soil. Ultimately, more fosthiazate was concentrated around the root, thereby exhibiting the satisfactory efficacy (Figure 6A and Table S4). This approach offers a strategy for the efficient utilization of potent hydrophilic pesticides in soil application scenarios.

By addressing the issue that fosthiazate has not been successfully microencapsulated and applied to practice, we proposed a strategy to regulate the structure of a shell of pesticide MCs. This work exemplifies a successful integration of micromechanism research and pesticide application scenarios. The strategy could also be extended to other pesticide varieties and application scenarios. For instance, the use of some nicotinoid pesticides has been restricted due to their negative effects on bee survival. Although microcapsules have the potential to mitigate the toxicity associated with pesticides, their high water solubility poses a challenge in terms of microencapsulation. Therefore, the elucidation of the encapsulation mechanism presented in this study offers a perspective for the advancement and application of pesticide microcapsules.

CONCLUSION

To investigate the influence of the characteristics of the core on MCs' formation and preparation stability, this study focuses on the influence of the shuttle effect at the interface induced by the hydrophilicity of the core on the shell structure. The mechanism underlying microcapsule formation at the nanoscale was elucidated by examining the impact of interfacial mass transfer on the interfacial condensation reaction. Furthermore, a strategy for regulating the microcapsule structure based on this mechanism was proposed. When the oil phase exhibited hydrophilicity, it enhanced the interfacial shuttle effect, leading to an increased depth of occurrence for the interfacial cross-linking reaction and resulting in the formation of loose and thick shells. However, in the presence of a hydrophobic substance within the oil phase, the interfacial polycondensation reaction exclusively takes place at the interface layer, resulting in the formation of a thin and compact shell. The shell thickness of MCs-SOL was 264 nm, only 19.13% compared to that of MCs-P2S1. The increased compactness of the shell resulted in a delayed release of fosthiazate and a reduction in the leaching distance. The release rate of the MCs-SOL sample in the release solution for 3 h is only 62.05%, and the leaching distance in the soil column is 8 cm. A large amount of active ingredient accumulated around the roots of crops is beneficial to improve the control efficacy to root galling nematode disease. Therefore, the control efficacy of the MCs-SOL samples in the field was as high as 87.3%. Incorporation of hydrophobic solvents into the core weakened the interfacial shuttle effect while enhancing shell compactness, reducing environmental risks, and improving application performance of the MCs. Moreover, this research complements existing theories on interfacial polymerization while proposing an efficient approach for encapsulating hydrophilic pesticides.

MATERIALS AND METHODS

Chemical. The 95% fosthiazate technical was provided by Hebei Veyong Biochem Co., Ltd. (Hebei, China). The 91% phoxim technical was provided by Hubei Xianlong Chemical Industry Co., Ltd. (Hubei, China). The 10% fosthiazate granules (G) were provided by Shandong Heyi Biotechnology Co., Ltd. (Shandong, China). MDI (99% 4,4-diphenylmethane diisocyanate) was purchased from Wanhua Chemical Group Co., Ltd. (Shandong, China). Ethylene glycol diacetate (EGDA) and propylene glycol diacetate (PGDA) were purchased from Shandong Ruiyang Chemical Co., Ltd. (Shandong, China). Technical grade solvent oil 150# (SOL) was purchased from Jinan Yinrun Chemical Co., Ltd. (Jinan, China). Sodium lignosulfonate (molecular weights: (1.0−1.2) × 10^4) was purchased from MeadWestvaco Inc. (United States) as a dispersing agent. The analytical grade *n*-hexane, methyl alcohol, absolute ethanol, and acetonitrile were purchased from Kermel Chemical Reagent Co., Ltd. (Tianjin, China).

https://doi.org/10.1021/acsnano.3c07915
ACS Nano XXXX, XXX, XXX−XXX

Preparation of Fosthiazate-Loaded MCs. The fosthiazate-loaded MCs were prepared via an interfacial polymerization. To prepare 100 g of fosthiazate-loaded MCs, 21.05 g of fosthiazate technical, 20 g of SOL, and 1.5 g of MDI were weighed and mixed to create a homogeneous oil phase. An aqueous phase consisting of 2 g of lignosulfonate and 55.45 g of deionized water was also prepared. The oil phase was then slowly poured into the aqueous phase and homogenized for 3 min at 25 °C. Different shearing speeds were employed to ensure the particle-size distributions of the fosthiazate oil-aqueous emulsions were similar. Subsequently, the emulsion was transferred to a glass bottle and stirred mechanically at 300 rpm for 3 h at 60 °C. Finally, deionized water was added to ensure that the fosthiazate content was 20%. Nine fosthiazate-loaded MCs samples were prepared using various solvents and shearing speeds, as shown in Table S1.

Characterization of Fosthiazate-Loaded MCs. The particle-size distribution of the MCs was evaluated by using a laser-based particle-size analyzer (LS-POP 6, Zhuhai OMEC Instrument Co., Ltd., China). The morphology of the MCs was observed using a scanning electron microscope (SEM, Phenom Pro, Phenom-World, Netherlands). The chemical composition of the MCs shell was detected by using a Fourier transform infrared spectrometer (FTIR) (TENSOR II, Bruker Optics, Germany). The thermal stability of fosthiazate-loaded MCs was tested using a thermogravimetric analyzer (TGA55, TA, USA), and this was repeated three times. The viscosity of the MCs samples was measured using a rotational viscometer and repeated three times (DV-III ULTRA, Brookfield, USA). The measurement of encapsulation efficiency and release behavior is detailed in Supporting Information.

Construction of the Oil-Aqueous Interface Evolution Model. An interface evolution model was developed to study the formation of the interface membrane at the oil-aqueous interface and the microprocess of shell formation for macro presentation. Table S2 presents the oil phase compositions of various treatments of the oil-aqueous interface model. First, add the oil phase to a 40 mL glass bottle. Then, water was slowly added to the glass bottle containing the oil phase to avoid disturbing the interface. At this point, there was a clear interface between the oil phases and aqueous phases. Place the glass bottle in a water bath environment of 25 ± 1 °C, and take photos after 3 h to record the changes in the oil-aqueous interface. After 3 h, oil phases and aqueous phases were sucked out by a syringe, and we slowly poured out the interfacial membrane. The membrane was dried at room temperature for 48 h, and its morphology was observed using SEM. The area of holes was calculated using ImageJ (Image Processing and Analysis in Java), and the area of holes was measured thrice for each treatment.

Mobility of Fosthiazate in Soil. The soil sample used for the leaching test is described in the Supporting Information. The method of pesticide mobility in soil was modified based on a previous report.[40] A device measuring 5 × 5 × 15 cm and filled with 220 g of sieved soil (60 mesh) was utilized. The 100 mL of 900 a.i. mg/L fosthiazate-loaded MCs diluent was added to a soil column using a constant current pump at a flow rate of 2 mL/min and allowed to stand for 24 h. After drying the soil, it was layered for testing the concentration of fosthiazate using the determined method described in the Supporting Information. The mobility experiments were repeated three times.

Field Experiment. To investigate the control efficacy of fosthiazate-loaded MCs on tomato root galling nematodes, a field experiment was conducted in a solar greenhouse in Dongdawu Village (Tai'an, P.R. China, 117.13 E, 35.98 N, 105 m above the mean sea level). The EC sample was used as a control. The dosage (active ingredient) of 20% fosthiazate-loaded MCs agent and 10% fosthiazate EC were both 80 a.i. mg/plant. Water was used as a blank control, and all samples were applied through root irrigation. Each treatment was repeated three times by using a completely randomized block design. Specific field experiment methods and bioactivity experiments are listed in the Supporting Information.

Data Analysis. The data analyses in this study were conducted using the Statistical Package for Social Sciences (SPSS) version 16.0 software. The standard error displayed as the mean was calculated using Tukey's multiple range test ($p < 0.05$). The curve-fitting analysis was conducted using Origin 2018.

ASSOCIATED CONTENT

Supporting Information

The Supporting Information is available free of charge at https://pubs.acs.org/doi/10.1021/acsnano.3c07915.

The method of encapsulation efficiency of fosthiazate-loaded MCs, the release profile of fosthiazate-loaded MCs, determined the concentration of fosthiazate in soil, degradation of fosthiazate in soil and bioactivity test. The information on tested soil and the grading standard and calculation formula of root-knot. Tables S1−S4, Figures S1−S7 (PDF)

Supporting movie S1 (MP4)

Supporting movie S2 (MP4)

Supporting movie S3 (MP4)

AUTHOR INFORMATION

Corresponding Authors

Feng Liu − *Department of Plant Protection, Shandong Agricultural University, Tai'an, Shandong 271018, People's Republic of China;* orcid.org/0000-0002-0271-3632; Email: fliu@sdau.edu.cn

Da-xia Zhang − *Department of Plant Protection, Shandong Agricultural University, Tai'an, Shandong 271018, People's Republic of China;* orcid.org/0000-0003-4846-4165; Email: daxia586@163.com

Authors

Tao Zhang − *Department of Plant Protection, Shandong Agricultural University, Tai'an, Shandong 271018, People's Republic of China*

Hongzhen Sun − *Department of Plant Protection, Shandong Agricultural University, Tai'an, Shandong 271018, People's Republic of China*

Liyuan Yang − *Department of Plant Protection, Shandong Agricultural University, Tai'an, Shandong 271018, People's Republic of China*

Peng Zhang − *Department of Jinan Tianbang Chemical Co., Ltd, Jinan, Shandong 250101, People's Republic of China*

Yaozhong Zhang − *Department of Shandong Province Insistute for the Control of Agrochemicls, Jinan, Shandong 250100, People's Republic of China*

Jingbo Bai − *Department of Shandong Siyuan Agricultural Development Co., Ltd, Zibo, Shandong 255400, People's Republic of China*

Complete contact information is available at: https://pubs.acs.org/10.1021/acsnano.3c07915

Notes

The authors declare no competing financial interest.

ACKNOWLEDGMENTS

This work was supported by grants from the National Natural Science Foundation of China (No. 32272596), Taishan Industrial Leading Talent Project (No. tscx202211021), and Modern Agricultural Industry Technology System for Vegetables in Shandong Province (No. SDAIT-05). We thank all those who have provided assistance and advice to this work and manuscript.

REFERENCES

(1) Chariou, P. L.; Steinmetz, N. F. Delivery of pesticides to plant parasitic nematodes using tobacco mild green mosaic virus as a nanocarrier. *ACS Nano* **2017**, *11*, 4719−4730.

(2) Malandrakis, A. A.; Kavroulakis, N.; Chrysikopoulos, C. V. Use of copper, silver and zinc nanoparticles against foliar and soil-borne plant pathogens. *Science of The Total Environment* **2019**, *670*, 292−299.

(3) Leong, W. H.; Teh, S. Y.; Hossain, M. M.; Nadarajaw, T.; Zabidi-Hussin, Z.; Chin, S. Y.; Lai, K. S.; Lim, S. H. E. Application, monitoring and adverse effects in pesticide use: The importance of reinforcement of Good Agricultural Practices (GAPs). *Journal of Environmental Management* **2020**, *260*, 109987.

(4) Zhang, C.; Hu, R.; Shi, G.; Jin, Y.; Robson, M. G.; Huang, X. Overuse or underuse? An observation of pesticide use in China. *Science of The Total Environment* **2015**, *538*, 1−6.

(5) Jing, T. F.; Zhang, D. X.; Pan, S. H.; Liu, G.; Mu, W.; Hou, Y.; Liu, F. Phenyl isocyanate-Modified avermectin B1a improves the efficacy against plant-parasitic nematode diseases by facilitating its soil mobility. *ACS Sustainable Chem. Eng.* **2020**, *8*, 2310−2319.

(6) Kodešová, R.; Kočárek, M.; Kodeš, V.; Drábek, O.; Kozák, J.; Hejtmánková, K. Pesticide adsorption in relation to soil properties and soil type distribution in regional scale. *Journal of Hazardous Materials* **2011**, *186*, 540−550.

(7) Zhang, Q. Z.; Du, Y.; Yu, M. L.; Ren, L. R.; Guo, Y. F.; Li, Q. H.; Yin, M. M.; Li, X. L.; Chen, F. Controlled release of dinotefuran with temperature/pH-responsive chitosan-gelatin microspheres to reduce leaching risk during application. *Carbohydr. Polym.* **2022**, *277*, 118880.

(8) Berens, M. J.; Capel, P. D.; Arnold, W. A. Neonicotinoid Insecticides in Surface Water, Groundwater, and Wastewater Across Land-Use Gradients and Potential Effects. *Environ. Toxicol. Chem.* **2021**, *40*, 1017−1033.

(9) Xiang, K.; Wu, Y.; Li, S.; Chen, J.; Xu, M.; Dai, W.; Wang, J. Thermosensitive methylcellulose spray-dried microcapsules as a controlled release carrier for soil management. *Aust. J. Chem.* **2022**, *75*, 953−965.

(10) Zhang, D. X.; Du, J.; Wang, R.; Luo, J.; Jing, T. F.; Li, B. X.; Mu, W.; Liu, F.; Hou, Y. M. Core/Shell dual-responsive nanocarriers via iron-mineralized electrostatic self-assembly for precise pesticide delivery. *Adv. Funct. Mater.* **2021**, *31*, 2102027.

(11) Wang, R.; Liu, S.; Sun, F. S.; Yu, X.; Liu, X.; Li, B. X.; Mu, W.; Zhang, D. X.; Liu, F. Balance the rapid release of insecticide microcapsules using double-layer shielding effect when the foliar application. *Chemical Engineering Journal* **2023**, *455*, 140899.

(12) Asaturova, A. M.; Bugaeva, L. N.; Homyak, A. I.; Slobodyanyuk, G. A.; Kashutina, E. V.; Yasyuk, L. V.; Sidorov, N. M.; Nadykta, V. D.; Garkovenko, A. V. Bacillusvelezensis strains for protecting cucumber plants from root-knot nematode meloidogyne incognita in a greenhouse. *Plants* **2022**, *11*, 275.

(13) Zhang, W. P.; Sun, W. C.; Wang, Y.; Liu, H. M.; Zhang, S. A.; Dong, B.; Ji, X. X.; Qiao, K. Management of meloidogyne incognita on cucumber with a new nonfumigant nematicide fluopimomide. *Plant Disease* **2022**, *106*, 151−155.

(14) Liu, Y. K.; Liu, Y. J.; Yang, L. Y.; Zhang, T.; Jin, Y.; Liu, L. H.; Du, J.; Zhang, D. X.; Li, B. X.; Gao, C. J.; Liu, F. The effect of abamectin application in combination with agronomic measures on the control efficacy of cucumber root-knot nematodes and the cucumber yield. *Pest Management Science* **2023**, *79*, 3190−3199.

(15) Tian, X. L.; Zhao, X. M.; Zhao, S. Y.; Zhao, J. L.; Mao, Z. C. The biocontrol functions of bacillus velezensis strain Bv-25 against meloidogyne incognita. *Frontiers in Microbiology* **2022**, *13*, 843041.

(16) Wu, J. X.; Wang, K.; Zhang, H. Y. Residues and dissipation dynamics of fosthiazate in tomato and soil. *Bull. Environ. Contam. Toxicol.* **2012**, *89*, 664−668.

(17) Huang, B.; Wang, Q.; Guo, M. X.; Fang, W. S.; Wang, X. N.; Wang, Q. X.; Yan, D. D.; Ouyang, C. B.; Li, Y.; Cao, A. C. The synergistic advantage of combining chloropicrin or dazomet with fosthiazate nematicide to control root-knot nematode in cucumber production. *Journal of Integrative Agriculture* **2019**, *18*, 2093−2106.

(18) Ma, T. Study on the process of 20% fosthiazate double layer microcapsule suspension agent *Chinese Academy of Agricultural Sciences* **2017**.

(19) Maruyama, T.; Ishibashi, Y.; Sano, M.; Taguchi, Y. Preparation and characterization of pesticide fosthiazate-loaded microcapsules for controlled release system. *Polym. Adv. Technol.* **2023**, *34*, 1133−1142.

(20) Jamekhorshid, A.; Sadrameli, S. M.; Farid, M. A review of microencapsulation methods of phase change materials (PCMs) as a thermal energy storage (TES) medium. *Renewable and Sustainable Energy Reviews* **2014**, *31*, 531−542.

(21) Pan, S. H.; Cao, H. C.; Li, B. X.; Zhang, D. X.; Mu, W.; Liu, F. Improving the efficacy against crop foliage disease by regulating fungicide adhesion on leaves with soft microcapsules. *Pest Management Science* **2021**, *77*, 4418−4424.

(22) Ma, D. C.; Zhang, T.; Wang, G. X.; Cao, C.; Mu, W.; Li, B. X.; Dou, D. L.; Liu, F. Polyurea microcapsule encapsulation improves the contact toxicity, inhibition time and control effect of trans-2-hexenal against Fusarium graminearum. *Industrial Crops and Products* **2023**, *195*, 116463.

(23) Meng, Q. Y.; Zhong, S. L.; Wang, J.; Gao, Y.; Cui, X. J. Advances in chitosan-based microcapsules and their applications. *Carbohydr. Polym.* **2023**, *300*, 120265.

(24) Li, L. H.; Cen, J.; Huang, L. L.; Luo, L.; Jiang, G. Q. Fabrication of a dual pH-responsive and photothermal microcapsule pesticide delivery system for controlled release of pesticides. *Pest Management Science* **2023**, *79*, 969−979.

(25) Luo, J.; Huang, X. P.; Jing, T. F.; Zhang, D. X.; Li, B.; Liu, F. Analysis of particle size regulating the insecticidal efficacy of phoxim polyurethane microcapsules on leaves. *ACS Sustainable Chem. Eng.* **2018**, *6*, 17194−17203.

(26) Song, Y. J.; Sun, P.; Henry, L.; Sun, B. H. Mechanisms of structure and performance controlled thin film composite membrane formation via interfacial polymerization process. *J. Membr. Sci.* **2005**, *251*, 67−79.

(27) Freger, V. Kinetics of film formation by interfacial polycondensation. *Langmuir.* **2005**, *21*, 1884−1894.

(28) Hu, Y. X.; Liu, Z. P.; Yuan, X. G.; Zhang, X. R. Molecular mechanism for liquid−liquid extraction: Two-film theory revisited. *AIChE J.* **2017**, *63*, 2464−2470.

(29) Aburabie, J.; Peinemann, K. V. Crosslinked poly(ether block amide) composite membranes for organic solvent nanofiltration applications. *J. Membr. Sci.* **2017**, *523*, 264−272.

(30) He, Z. L.; Jiang, S.; Li, Q. F.; Wang, J. W.; Zhao, Y. H.; Kang, M. Q. Facile and cost-effective synthesis of isocyanate microcapsules via polyvinyl alcohol-mediated interfacial polymerization and their application in self-healing materials. *Compos. Sci. Technol.* **2017**, *138*, 15−23.

(31) Cao, H. C.; Zhang, D. X.; Liu, S.; Luo, J.; Jing, T.; Pan, S. H.; Liu, F.; Li, B. X.; Mu, W. Achieving win−win ecotoxicological safety and fungicidal activity of pyraclostrobin-loaded polyurea microcapsules by selecting proper polyamines. *J. Agric. Food Chem.* **2021**, *69*, 2099−2107.

(32) Xiao, D. X.; Liang, W. L.; Xie, Z. G.; Cheng, J. L.; Du, Y. J.; Zhao, J. H. A temperature-responsive release cellulose-based microcapsule loaded with chlorpyrifos for sustainable pest control. *Journal of Hazardous Materials* **2021**, *403*, 123654.

(33) Wei, J.; Liu, X.; Qiu, C.; Wang, R.; Tang, C. Y. Influence of monomer concentrations on the performance of polyamide-based thin film composite forward osmosis membranes. *J. Membr. Sci.* **2011**, *381*, 110−117.

(34) Cao, H. C.; Chen, Y.; Zhang, D. X.; Jin, Y.; Zhang, P.; Li, B. X.; Mu, W.; Liu, F. Octaphenyl polyoxyethylene regulates the flexibility of pyraclostrobin-loaded soft microcapsules by interfacial polymerization for better foliar adhesion and pesticide utilization. *Chemical Engineering Journal* **2022**, *439*, 135805.

(35) Zhang, R. J.; Yu, S. L.; Shi, W. X.; Zhu, J. Y.; Van der Bruggen, B. Support membrane pore blockage (SMPB): An important

https://doi.org/10.1021/acsnano.3c07915
ACS Nano XXXX, XXX, XXX−XXX

phenomenon during the fabrication of thin film composite membrane via interfacial polymerization. *Sep. Purif. Technol.* **2019**, *215*, 670−680.
(36) Chen, L.; Zhang, M. J.; Zhang, S. Y.; Shi, L.; Yang, Y. M.; Liu, Z.; Ju, X. J.; Xie, R.; Wang, W.; Chu, L. Y. Simple and continuous fabrication of self-propelled micromotors with photocatalytic metal−organic frameworks for enhanced synergistic environmental remediation. *ACS Appl. Mater. Interfaces* **2020**, *12*, 35120−35131.
(37) Luo, J.; Zhang, D. X.; Jing, T. F.; Liu, G.; Cao, H. C.; Li, B. X.; Hou, Y. M.; Liu, F. Pyraclostrobin loaded lignin-modified nanocapsules: Delivery efficiency enhancement in soil improved control efficacy on tomato Fusarium crown and root rot. *Chemical Engineering Journal* **2020**, *394*, 124854.
(38) Zhang, X. P.; Zhang, L. X.; Zhang, D. X.; Liu, S. S.; Wei, D. G.; Liu, F. Mechanism of the temperature-responsive material regulating porous morphology on epoxy phenolic novolac resin microcapsule surface. *Colloids Surf., A* **2020**, *593*, 124581.
(39) Jing, T. F.; Zhang, D. X.; Zhang, Y. Z.; Jin, Y.; Han, X. Z.; Mu, W.; Li, B. X.; Liu, F. Adsorption behaviour and mechanism of avermectin-based pesticides in soil driven by H-bonds formed between the compounds and humus. *Chemical Engineering Journal* **2023**, *459*, 141647.
(40) Du, J.; Wang, C. L.; Liu, Y. K.; Xue, C. B.; Ge, J. C.; Si, G. D.; Han, X. Z.; Liu, F.; Zhang, D. X.; Li, B. X. One-pot construction of epoxy resin nanocarrier delivering abamectin and its efficacy on plant root-knot nematodes. *Pest Management Science* **2023**, *79*, 3103−3113.

https://doi.org/10.1021/acsnano.3c07915
ACS Nano XXXX, XXX, XXX−XXX